Article
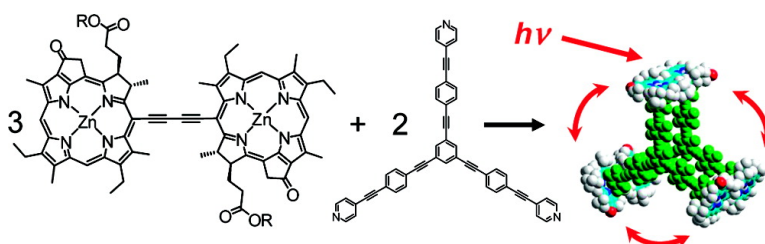
Intramolecular Energy Transfer within Butadiyne-Linked Chlorophyll and Porphyrin Dimer-Faced, Self-Assembled Prisms

Richard F. Kelley, Suk Joong Lee, Thea M. Wilson, Yasuyuki Nakamura,
David M. Tiede, Atsuhiro Osuka, Joseph T. Hupp, and Michael R. Wasielewski

More About This Article

Additional resources and features associated with this article are available within the HTML version:

- Supporting Information
- Links to the 4 articles that cite this article, as of the time of this article download
- Access to high resolution figures
- Links to articles and content related to this article
- Copyright permission to reproduce figures and/or text from this article

View the Full Text HTML

Intramolecular Energy Transfer within Butadiyne-Linked Chlorophyll and Porphyrin Dimer-Faced, Self-Assembled Prisms

Richard F. Kelley,[†,‡] Suk Joong Lee,[†,‡] Thea M. Wilson,[†,‡] Yasuyuki Nakamura,[||]
David M. Tiede,*[,‡,§] Atsuhiro Osuka,*[,||] Joseph T. Hupp,*[,†,‡] and
Michael R. Wasielewski*[,†,‡]

Department of Chemistry and Argonne-Northwestern Solar Energy Research (ANSER) Center, Northwestern University, Evanston, Illinois 60208-3113, Chemistry Division, Argonne National Laboratory, Argonne, Illinois 60439, and Department of Chemistry, Graduate School of Science, Kyoto University, Kyoto 606-8502, Japan

Received July 23, 2007; E-mail: m-wasielewski@northwestern.edu

Abstract: The synthesis and photophysical properties of butadiyne-linked chlorophyll and porphyrin dimers in toluene solution and in several self-assembled prismatic structures are described. The butadiyne linkage between the 20-positions of the macrocycles results in new electronic transitions polarized along the long axes of the dimers. These transitions greatly increase the ability of these dimers to absorb the solar spectrum over a broad wavelength range. Femtosecond transient absorption spectroscopy reveals the relative rate of rotation of the macrocycles around the butadiyne bond joining them. Following addition of 3-fold symmetric, metal-coordinating ligands, both macrocyclic dimers self-assemble into prismatic structures in which the dimers comprise the faces of the prisms. These structures were confirmed by small-angle X-ray scattering experiments in solution using a synchrotron source. Photoexcitation of the prismatic assemblies reveals that efficient, through-space energy transfer occurs between the macrocyclic dimers within the prisms. The distance dependence of energy transfer between the faces of the prisms was observed by varying the size of the prismatic assemblies through the use of 3-fold symmetric ligands having arms with different lengths. These results show that self-assembly of discrete macrocyclic prisms provides a useful new strategy for controlling singlet exciton flow in antenna systems for artificial photosynthesis and solar cell applications.

Introduction

Photofunctional materials for use in organic photovoltaics must be capable of transferring energy efficiently due to the relatively long distances photogenerated excitons must travel to reach the interface at which charge carriers are generated.[1,2] Several studies have examined multiporphyrin arrays constructed with ethynyl and butadiynyl linkers for applications in photovoltaic devices.[3,4] The linkers in these arrays provide extended conjugation between the macrocycles resulting in new, low-energy electronic transitions, which provide enhanced solar spectral absorption. The same studies, however, have also shown these linkers allow rotational conformational heterogeneity, which can diminish the population of molecules having the desired low-energy transition. To address this problem, another recent study introduced a bridging ligand into a solution of butadiyne-linked porphyrin arrays to coordinate to the porphyrin metal centers, thus locking the chromophores in a rigid, oriented fashion.[5] The strain induced by the coordinating ligand caused the chromophores to deviate from planarity by bending the butadiyne linkage. This bending may result in disorder if the systems were to be incorporated into solid-phase devices. Coordination bond formation between tetrapyrrole metal centers and polydentate ligands is an attractive strategy for building supramolecular structures in which the chromophores are planarized as the result of coordination. This coordination-driven self-assembly strategy has become a very successful method for constructing a variety of 3-D supermolecules.[6–22] Increasing the number of coordination bonding sites within the structure

[†] Department of Chemistry, Northwestern University.
[‡] ANSER Center, Northwestern University.
[§] Chemistry Division, Argonne National Laboratory.
[||] Graduate School of Science, Kyoto University.
(1) Haugeneder, A.; Neges, M.; Kallinger, C.; Spirkl, W.; Lemmer, U.; Feldmann, J.; Scherf, U.; Harth, E.; Gügel, A.; Müllen, K. *Phys. Rev. B: Condens. Matter* **1999**, *59*, 15346−15351.
(2) Peumans, P.; Yakimov, A.; Forrest, S. R. *J. Appl. Phys.* **2003**, *93*, 3693−3723.
(3) Kumble, R.; Palese, S.; Lin, V. S. Y.; Therien, M. J.; Hochstrasser, R. M. *J. Am. Chem. Soc.* **1998**, *120*, 11489−11498.
(4) Ahn, T. K.; Yoon, Z. S.; Hwang, I.-W.; Lim, J. K.; Rhee, H.; Joo, T.; Sim, E.; Kim, S. K.; Aratani, N.; Osuka, A.; Kim, D. *J. Phys. Chem. B* **2005**, *109*, 11223−11230.

(5) Winters, M. U.; Kaernbratt, J.; Eng, M.; Wilson, C. J.; Anderson, H. L.; Albinsson, B. *J. Phys. Chem. C* **2007**, *111*, 7192−7199.
(6) Tabushi, I.; Kugimiya, S.; Kinnaird, M. G.; Sasaki, T. *J. Am. Chem. Soc.* **1985**, *107*, 4192−4199.
(7) Hunter, C. A.; Meah, M. N.; Sanders, J. K. M. *J. Chem. Soc., Chem. Commun.* **1988**, 694−696.
(8) Hunter, C. A.; Leighton, P.; Sanders, J. K. M. *J. Chem. Soc., Perkin Trans.* **1989**, *1*, 547−552.
(9) Camara-Campos, A.; Hunter, C. A.; Tomas, S. *Proc. Natl. Acad. Sci. U.S.A.* **2006**, *103*, 3034−3038.
(10) Ballester, P.; Oliva, A. I.; Costa, A.; Deya, P. M.; Frontera, A.; Gomila, R. M.; Hunter, C. A. *J. Am. Chem. Soc.* **2006**, *128*, 5560−5569.
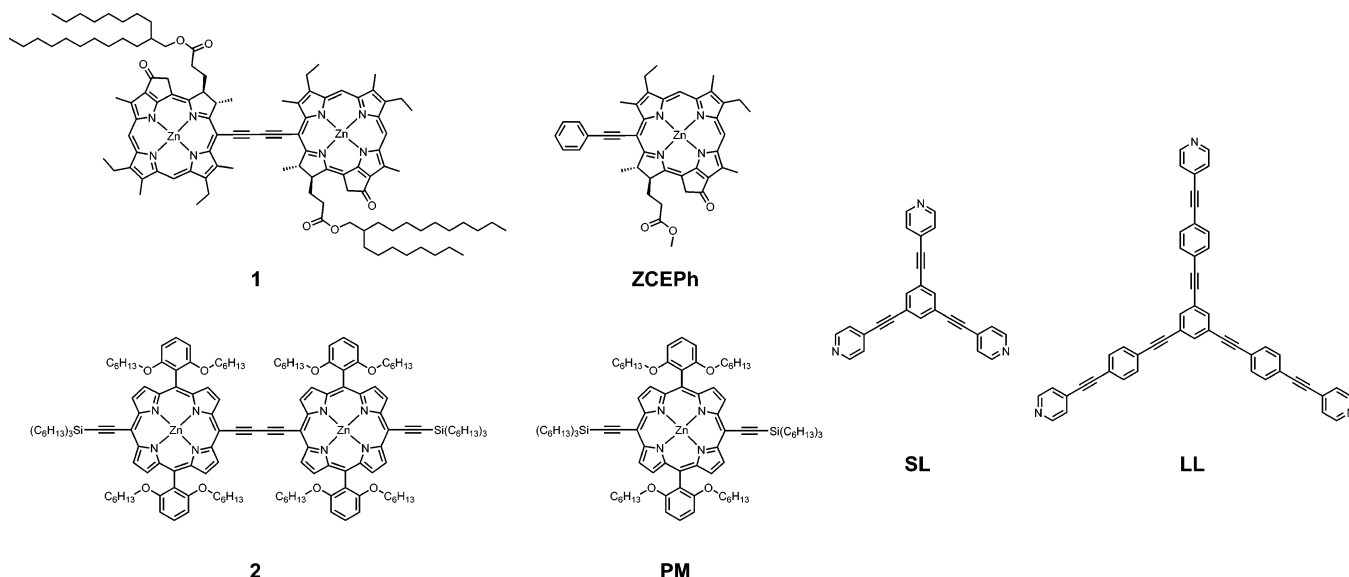
Figure 1. Structures of the molecules in this study.

enhances cooperative effects and increases control over the assembly geometry. We recently reported on a supramolecular architecture in which the combination of butadiyne-linked porphyrins with triethynylpyridylbenzene resulted in the reversible formation of trigonal, prismatic assemblies.[23] In addition to fixing the butadiyne-linked chromophores in the red-absorbing, planar orientation, the prismatic architecture provides a 3-dimensional structure that can potentially be used to bias the orientation of the structures in the solid phase. The ability to control aggregate assembly is beneficial in photovoltaic applications, where efficient energy transfer is required, yet often limited by molecular disorder. The presence of multiple chromophores within close proximity allows for ultrafast energy migration to occur between faces of the prisms. We have also recently developed the methodology for attaching ethynyl linkers directly to the macrocyclic cores of chlorophyll *a* derivatives.[24] The electronic asymmetry inherent in the chlorin chromophore, resulting from the reduced D-ring, enhances the intensity of the Q_y transition. By incorporation of chlorophyll into butadiyne-linked dimers, the oscillator strength of the transition polarized along the butadiyne axis is also enhanced. We now report the structural characterization and photophysics of butadiyne-linked chlorophyll and porphyrin dimers as well as several self-assembled prisms comprised of them in toluene solution.

Experimental Section

The synthesis and characterization of **1** and **LL** (Figure 1) are described in detail in the Supporting Information, while that of **2**, **PM**, **ZCEPh**, and **SL** were previously reported.[23,25] Characterization was performed with a Varian 400 MHz NMR and PE Voyager DE-Pro MALDI-TOF mass spectrometers. High-resolution electrospray and fast atom bombardment mass spectra were obtained with the 70-SE-4F and Q-Tof Ultima mass spectrometers at the University of Illinois at Urbana-Champaign.
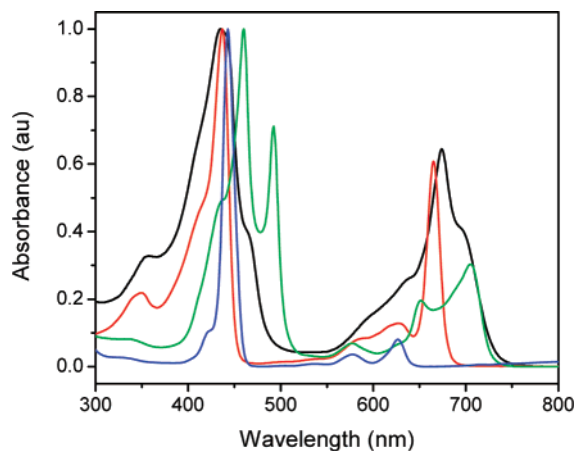
UV−vis absorption measurements were made on a Shimadzu spectrometer (UV1601). Steady-state fluorescence measurements were made on a single photon counting fluorometer (PTI). All measurements were performed at room temperature. Fluorescence studies of the dimers were conducted on solutions with optical densities below 0.1 at the absorption maxima in a 1-cm cuvette using right angle excitation/emission geometry. Fluorescence studies of the prisms were conducted on solutions with optical densities above 0.3 at the absorption maxima in a 2-mm cuvette to ensure that the samples existed in their prismatic states, and front-face fluorescence spectra were collected. Toluene was purified by passing it through a series of CuO and alumina columns immediately prior to use.

X-ray scattering measurements were carried out using the undulator beam line 12-ID at the Advanced Photon Source (APS), Argonne National Laboratory. The X-ray scattering instrument utilized a double-crystal Si(111) monochromator and a two-dimensional mosaic CCD detector.[26] The X-ray wavelength was set at $\lambda = 0.62$ Å, and the sample to detector distance was adjusted to achieve scattering measured across the 0.007 Å$^{-1} < q < 0.27$ Å^{-1} region, where $q = (4\pi/\lambda) \sin \theta$, λ is the X-ray scattering wavelength, and 2θ is the scattering angle. Quartz capillaries (2 mm diameter) were used as sample containers. All samples were filtered through 200 nm PTFE filters (Whatman) prior to the measurements. The scattering intensity was averaged over 300 measurements, after which the solvent scattering intensity was analogously measured and subtracted from the sample spectrum.

(11) Ballester, P.; Costa, A.; Deya, P. M.; Frontera, A.; Gomila, R. M.; Oliva, A. I.; Sanders, J. K. M.; Hunter, C. A. *J. Org. Chem.* **2005**, *70*, 6616−6622.

(12) Ballester, P.; Costa, A.; Castilla, A. M.; Deya, P. M.; Frontera, A.; Gomila, R. M.; Hunter, C. A. *Chem.−Eur. J.* **2005**, *11*, 2196−2206.

(13) Ogawa, K.; Kobuke, Y. *J. Photochem. Photobiol., C* **2006**, *7*, 1−16.

(14) Nakagawa, H.; Ogawa, K.; Satake, A.; Kobuke, Y. *Chem. Commun. (Cambridge, U.K.)* **2006**, 1560−1562.

(15) Hajjaj, F.; Yoon, Z. S.; Yoon, M.-C.; Park, J.; Satake, A.; Kim, D.; Kobuke, Y. *J. Am. Chem. Soc.* **2006**, *128*, 4612−4623.

(16) Furutsu, D.; Satake, A.; Kobuke, Y. *Inorg. Chem.* **2005**, *44*, 4460−4462.

(17) Anderson, H. L. *Chem. Commun.* **1999**, 2323−2330.

(18) Taylor, P. N.; Anderson, H. L. *J. Am. Chem. Soc.* **1999**, *121*, 11538−11545.

(19) Drobizhev, M.; Stepanenko, Y.; Rebane, A.; Wilson, C. J.; Screen, T. E. O.; Anderson, H. L. *J. Am. Chem. Soc.* **2006**, *128*, 12432−12433.

(20) Screen, T. E. O.; Thorne, J. R. G.; Denning, R. G.; Bucknall, D. G.; Anderson, H. L. *J. Am. Chem. Soc.* **2002**, *124*, 9712−9713.

(21) Dy, J. T.; Ogawa, K.; Satake, A.; Ishizumi, A.; Kobuke, Y. *Chem.−Eur. J.* **2007**, *13*, 3491−3500, S3491/3491−S3491/3498.

(22) Hoffmann, M.; Wilson, C. J.; Odell, B.; Anderson, H. L. *Angew. Chem., Int. Ed.* **2007**, *46*, 3122−3125.

(23) Lee, S. J.; Mulford, K. L.; O'Donnell, J. L.; Zuo, X.; Goshe, A. J.; Wesson, P. J.; Nguyen, S. T.; Hupp, J. T.; Tiede, D. M. *Chem. Commun. (Cambridge, U.K.)* **2006**, 4581−4583.

(24) Kelley, R. F.; Tauber, M. J.; Wasielewski, M. R. *J. Am. Chem. Soc.* **2006**, *128*, 4779−4791.

(25) Kelley, R. F.; Tauber, M. J.; Wasielewski, M. R. *Angew. Chem., Int. Ed.* **2006**, *45*, 7979−7982.

(26) Seifert, S.; Winans, R. E.; Tiede, D. M.; Thiyagarajan, P. *J. Appl. Crystallogr.* **2002**, *33*, 782−784.

Figure 2. Ground-state absorption spectra of **1** (black), **ZCEPh** (red), **PM** (blue), and **2** (green) in toluene.
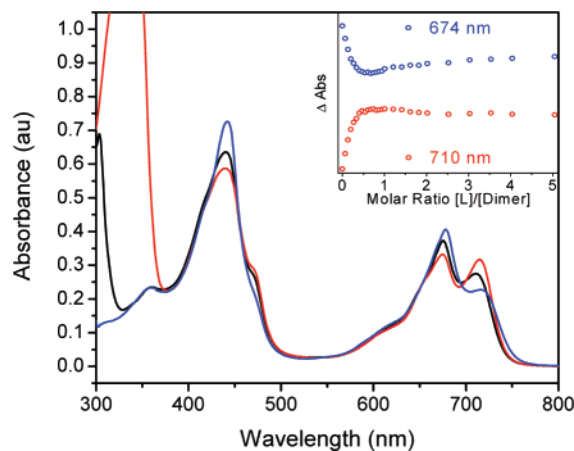
Femtosecond transient absorption measurements were made using a Ti:sapphire laser system as detailed in the Supporting Information. The instrument response function (IRF) for the pump−probe experiments was 150 fs. Typically 5 s of averaging was used to obtain the transient spectrum at a given delay time. Quartz cuvettes with a 2 mm path lengths were used, and the samples were irradiated with 0.1−1.0 μJ pulses focused to a 200-μm diameter spot. The optical density at λ_{ex} was kept between 0.4 and 0.8. Analysis of the kinetic data was performed at multiple wavelengths using a Levenberg−Marquardt nonlinear least-squares fit to a general sum-of-exponentials function with an added Gaussian to account for the finite instrument response.

Fluorescence lifetime measurements were performed using a frequency-doubled, cavity-dumped Ti:sapphire laser as the excitation source and a Hamamatsu C4780 picosecond fluorescence lifetime measurement system as described in the Supporting Information. The energy of the 400 nm, 25 fs pulses was attenuated to approximately 1.0 nJ/pulse for all fluorescence lifetime experiments. The total IRF of the streak camera system was 20 ps. The samples were prepared in 2 mm path length quartz cuvettes, and time-resolved data were collected for each sample at the same concentrations and experimental orientations as the steady-state data. All fluorescence data was acquired in single photon counting mode using the Hamamatsu HPD-TA software. The data was fit using the Hamamatsu fitting module and deconvoluted using the laser pulse profile.

Results and Discussion

Synthesis. Homocoupling of zinc 2-octyl-1-dodecyl 3-ethyl-20-ethynylpyrochlorophyllide *a*[25] using Glaser-Hay methodology[23] provided **1** in 50% yield. Two sequential Sonogashira cross-coupling reactions[27] were used to synthesize **LL**. The first coupling, between 4-ethynylpyridine and 1,4-dibromobenzene, resulted in the formation of 4-(4-bromophenylethynyl)pyridine, in 72% yield. The second coupling, between 4-(4-bromophenylethynyl)pyridine and 1,3,5-triethynylbenzene,[28] resulted in **LL** in 59% yield. The synthesis and characterization of zinc methyl 3-ethyl-20-phenylethynylpyrochlorophyllide *a* (**ZCEPh**), **2**, porphyrin monomer (**PM**), and **SL** were reported previously.[23,25]

Steady-State Spectroscopy. The ground-state absorption spectra of **1**, **ZCEPh**, **2**, and **PM** in toluene are compared in Figure 2. The spectrum of **ZCEPh** displays a Soret band at 435 nm and Q bands at 578, 628, and 665 nm, typical of zinc

(27) Wagner, R. W.; Johnson, T. E.; Li, F.; Lindsey, J. S. *J. Org. Chem.* **1995**, *60*, 5266−5273.
(28) Mongin, O.; Papamicael, C.; Hoyler, N.; Gossauer, A. *J. Org. Chem.* **1998**, *63*, 5568−5580.

Figure 3. Ground-state absorption spectra of **1₃-SL₂** in toluene (black), **1₃-LL₂** in toluene (red), and **1** in pyridine (blue). Inset: Spectrophotometric titration curves of **1₃-SL₂** in toluene (1.3×10^{-5} M) at 674 and 710 nm.

chlorophyllide species. The spectrum of **1** is considerably broadened, and its Q bands are red-shifted relative to **ZCEPh** with its Soret band at 436 nm and Q bands at 596, 638, and 674 nm. In addition to the expected absorption bands, new spectral features are observed at 469 and 694 nm. While the red shifting is due to the increase in conjugation length of the chlorophyll π-system, the spectral features at 469 and 694 are indicative of new allowed transitions. Similar transitions have been observed in ethynyl- and butadiynyl-linked porphyrin dimers and are attributed to an electronic transition that is polarized along the long axis of the molecules.[3−5] In the **PM** spectrum, the porphyin Soret band is observed at 443 nm and the Q bands appear at 537, 578, and 627 nm. In the spectrum of **2**, the porphyin Soret band is split into three separate bands, observed at 438, 460, and 493 nm, and the Q bands appear at 577, 652, and 705 nm. The red-shift and increase in amplitude of the Q-bands is indicative of further reduction of the electronic symmetry within both component chromophores and electronic delocalization along the long axis of the dimer.[18,29,30] It is interesting to note that while the electronic spectrum of the porphyrin monomer and dimer differ significantly, the chlorophyll dimer retains its $Q_y(0,0)$ transition. Despite the differences between the absorption features of the component chromophores, the lowest energy absorption features for both dimers occur at surprisingly similar energies.
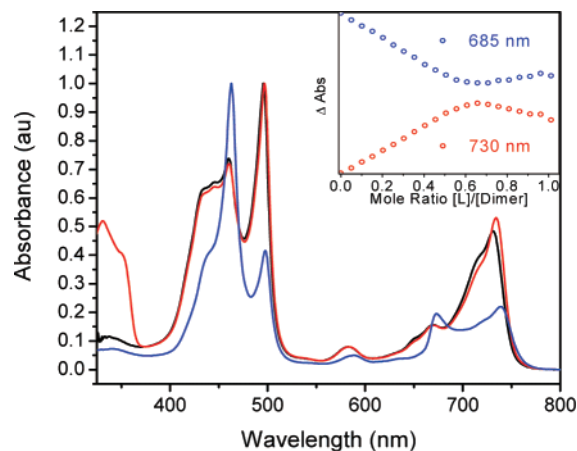
The spectrophotometric titration of **SL** into a toluene solution of **1** revealed a new species of **1** with a lower intensity Soret band, red-shifted to 440 nm, and the lowest energy Q bands broadened and red-shifted to 676 and 712 nm, Figure 3. The intensity of the lowest energy absorption feature reached a maximum following the net addition of 2/3 equiv of **SL** to **1**, Figure 3 inset. Following the continued addition of **SL**, the features of this intermediate species transition into those observed in a pyridine solution of **1**, which displays a Soret band at 442 nm and low-energy Q bands occurring at 678 and 716 nm. The titration reveals that the observed binding stoichiometry of the intermediate species is consistent with the formation of the proposed prism, **1₃-SL₂**, and the enhancement of the lowest energy absorption band spectrum of the intermedi-

(29) Anderson, H. L. *Inorg. Chem.* **1994**, *33*, 972−981.
(30) LeCours, S. M.; DiMagno, S. G.; Therien, M. J. *J. Am. Chem. Soc.* **1996**, *118*, 11854−11864.

Figure 4. Ground-state absorption spectra of 2_3-SL_2 in toluene (black), 2_3-LL_2 in toluene (red), and **2** in pyridine (blue). Inset: Spectrophotometric titration curves of 2_3-SL_2 in toluene (3.1×10^{-6} M) at 685 and 730 nm.

ate state is consistent with the planar conformation of **1** in a prismatic assembly.[23] The titration data for **1** and **SL** was fit to a three-chromophore model using multivariate factor analysis to obtain the equilibrium constant $K_{32} = (2.27 \pm 0.09) \times 10^{24}$ M^{-4} for formation of 1_3-SL_2 (see Supporting Information, Figures S1−S3) These results suggest that the 1_3-SL_2 prism is fully formed and stable after the stoichiometric addition of 2/3 equiv of SL and that the prismatic assembly is maintained under the conditions used for the photophysical measurements (see also SAXS data given below).

The addition of 2/3 equiv of **LL** to a toluene solution of **1** resulted in an additional decrease in the intensity its Soret band and red shifting of its Q bands to 675 and 715 nm, Figure 3. The lowest energy Q-band also increased in intensity at the expense of the higher energy band. The intensity differences between the Q bands in the prisms constructed from **SL** and **LL** are attributed to the degree of planarization within the dimers.[18] With the larger trigonal ligand, there is less steric hindrance between the dimers in the prisms and the chromophoric subunits within the dimers are most likely able to adopt a more planar geometry relative to one another.

The spectrophotometric titration yielding 2_3-SL_2 in toluene, the spectrum resulting from the addition of 2/3 equiv of **LL** to a toluene solution of **2**, and the spectrum of **2** in pyridine are presented in Figure 4. A detailed explanation of the spectrum of 2_3-SL_2 in toluene was previously reported.[23] The spectrum of 2_3-LL_2 also displays a decrease in the intensity of the highest energy Soret band of **2** and red shifting of the lowest energy Q bands to 734 nm (Figure 4). The intensity differences between the Q bands of the two porphyrin prisms are smaller than those of the chlorophyll prisms indicating that the degree of planarization within the porphyrin dimers does not change as much with the different trigonal ligands.

Exciton coupling between the dimers that comprise the faces of the prisms results from the orientation of their transition dipole moments, which are aligned parallel to the long molecular axis of each dimer.[31] The parallel geometry results in blue shifting of the absorption features of the dimers within the prisms relative to those of disaggregated **1** and **2** in pyridine.[31] The magnitude of exciton splitting between the dimers is

(31) Kasha, M.; Rawles, H. R.; El-Bayoumi, M. L. *Pure Appl. Chem* **1965**, *11*, 371−392.
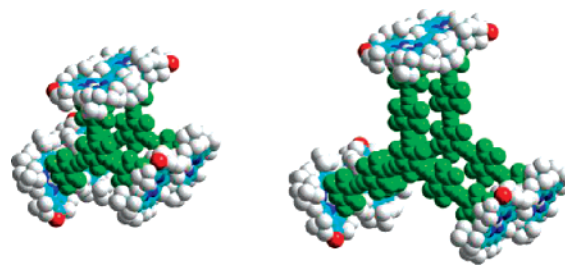
Figure 5. MM+ geometry-optimized models for 1_3-SL_2 (left) and 1_3-LL_2 (right).

inversely proportional to the distance between their dipoles cubed.[32,33] Therefore, the longer distances between the chromophores in 1_3-LL_2 and 2_3-LL_2 result in the smaller splittings observed in their absorption features relative to those in 1_3-SL_2 and 2_3-SL_2.

Small-Angle X-ray Scattering. To confirm the prismatic structures of 1_3-SL_2, 1_3-LL_2, and 2_3-LL_2, small-angle X-ray scattering (SAXS) measurements were performed on 10^{-4} M toluene solutions using a high-flux synchrotron source (Advanced Photon Source at Argonne National Laboratory). Similar studies of 2_3-SL_2 in toluene solution were previously reported.[23] Solution-phase scattering patterns of 1_3-SL_2, 1_3-LL_2, and 2_3-LL_2 in toluene were obtained over the q region 0.007 Å^{-1} < q < 0.27 Å^{-1}. In the low-resolution scattering region (q < 0.2 Å^{-1}), the scattering intensity follows the Guinier relationship, $I(q) = I(0) \exp(-q^2 R_g^2/3)$, which is parametrized in terms of the forward scattering amplitude, $I(0)$, and the radius of gyration, R_g.[34,35] The linearity of the Guinier plot is a measure of structural dispersity.[36] The linear Guinier plots over the range 0.003 Å^{-2} < q^2 < 0.008 Å^{-2} indicate that 1_3-SL_2, 1_3-LL_2, and 2_3-LL_2 each have monodisperse structures, Figures S4−S6. The least-squares fit to the linear data reveal radii of gyration of 12.4, 16.7, and 17.9 Å for 1_3-SL_2, 1_3-LL_2, and 2_3-LL_2 respectively. MM+ geometry-optimized models for the prismatic structures were created using Hyperchem, Figure 5.[37] Coordinate-based scattering data were then generated for each model[38] and fit using the Guinier approximation in the same manner as the experimentally obtained data; see insets to Figures S4−S6. The R_g values obtained from the linear fits to the simulated data for the 1_3-SL_2, 1_3-LL_2, and 2_3-LL_2 models were 12.2, 16.9, and 18.1 Å, respectively. Given that the R_g values obtained from both the experiments and the prism models are nearly identical and that a 3:2 ratio of dimers to ligands is observed in the spectrophotometric titration data, we conclude that the aggregates found in toluene solution are trigonal prisms.

Transient Absorption Spectroscopy. Excitation of **1** in toluene with 710-nm, 120-fs pulses yields the transient absorption spectra shown in Figure 6 within the instrument response function of the apparatus. Negative features occur at 642, 675, and 705 nm and below 480 nm, while a broad positive feature

(32) Cantor, C. R.; Schimmel, P. R. *Biophysical Chemistry*; W. H. Freeman: New York, 1980; Vol. 2.
(33) Harada, N.; Nakanishi, K. *Circular dichroic spectroscopy: exciton coupling in organic stereochemistry*; University Science Books: Mill Valley, CA, 1983.
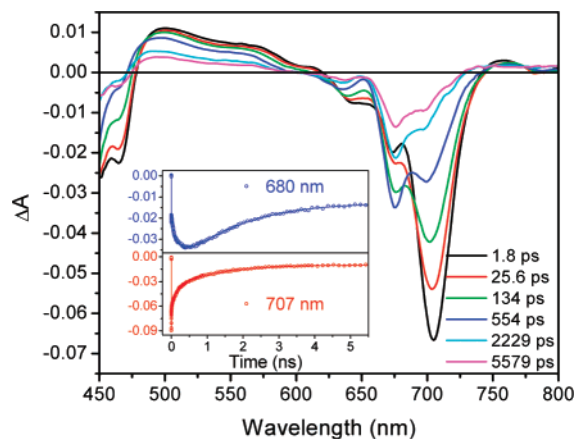(34) Glatter, O. *Neutron X-ray and Light Scattering*; Elsevier: Amsterdam, 1991.
(35) Guinier, A.; Fournet, G. *Small Angle Scattering*; Wiley: New York, 1955.
(36) Svergun, D. I.; Koch, M. H. J. *Rep. Prog. Phys.* **2003**, *66*, 1735−1782.
(37) *Hyperchem(TM)*; Hypercube Inc.: 1115 NW 4th Street, Gainesville, FL 32601.
(38) Zhang, R. T.; Thiyagarajan, P.; Tiede, D. M. *J. Appl. Crystallogr.* **2000**, *33*, 565−568.

Figure 6. Transient absorption spectra of **1** in toluene following excitation with 710-nm, 120-fs laser pulses. Inset: Transient absorption kinetics for **1** at (blue) 680 nm and at (red) 707 nm. Nonlinear least-squares fits to the data are also shown.
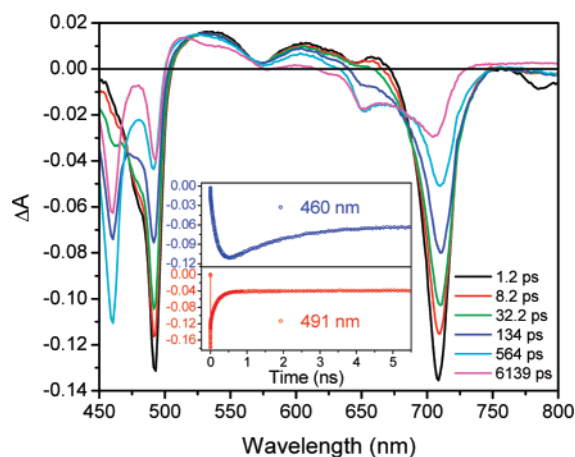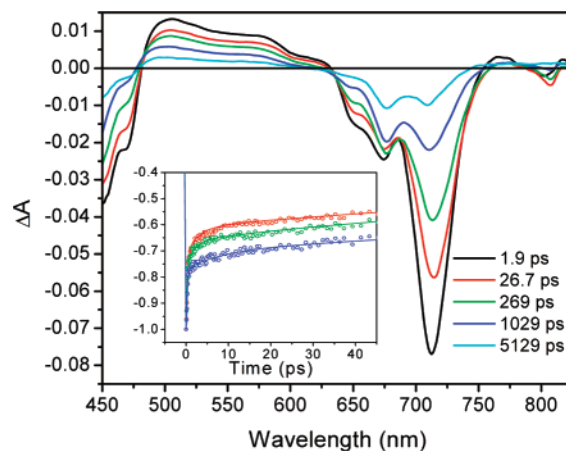

Figure 7. Transient absorption spectra of **2** in toluene following excitation with 705-nm, 120-fs laser pulses. Inset: Transient absorption kinetics for **2** at (blue) 460 nm and at (red) 491 nm. Nonlinear least-squares fits to the data are also shown.

is observed between 480 and 620 nm. These features decay over time to reveal bleaching that closely matches the inverted ground state absorption spectrum of **1** in toluene, with Q bands at 635, 676, and 697 nm, the Soret band below 470 nm, and a broad positive feature between 470 and 615 nm. Transient kinetics monitored at 680 and 707 nm, Figure 6 inset, show three exponential components with lifetimes (amplitudes) of 0.29 ± 0.05 ps (0.50), 176 ± 23 ps (0.22), and 1.2 ± 0.1 ns (0.28), respectively.

Excitation of **2** in toluene with 705-nm, 120-fs pulses yields negative features at 493 and 709 nm and a broad positive feature between 503 and 672 nm, Figure 7. These spectral features also decay over time to reveal negative features that closely match the inverted ground-state absorption spectrum of **2** in toluene, with Q bands at 625, 652, and 704 nm, the Soret bands at 460 and 493 nm, and a broad absorption feature between 501 and 614 nm. Transient kinetics monitored at 460 and 491 nm, Figure 7 inset, also show three exponential components with lifetimes of 0.11 ± 0.01 ps, 175 ± 16 ps, and 1.3 ± 0.1 ns, respectively. The corresponding amplitudes are 0.63, 0.06, and 0.31 at 460 nm and 0.61, 0.33, and 0.06 at 491 nm.

The initial negative absorption changes in the transient spectra of both **1** and **2** are nearly identical with the lowest energy
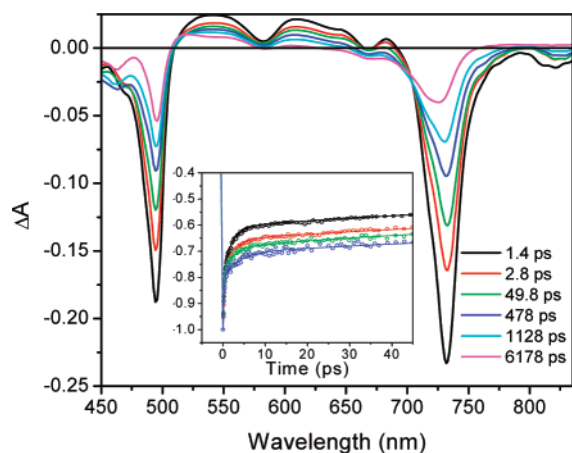

Figure 8. Transient absorption spectra of **1₃-SL₂** in toluene following excitation with 710-nm, 120-fs laser pulses. Inset: Power-dependent transient absorption kinetics monitored at 721 nm using 0.66 (red), 0.33 (green), and 0.11 (blue) μJ per 710 nm excitation pulse.

transitions observed in the ground-state absorption spectra of the prismatic assemblies, Figures 3 and 4. This suggests that the majority of the molecules excited by the wavelength-selective laser pulse are in the conformation where the chromophores are coplanar within the dimers. In this conformation, the electronic transition selectively excited is polarized along the butadiynyl axis. The first component in the transient kinetics of both dimers is the result of nonlinear decay processes made possible by the increased polarizability resulting from the extended conjugation of the coplanar macrocycles.[19,20,39] The second component is indicative of the torsional dynamics of the macrocycles as they rotate around the butadiyne linkage, from twisted conformations into the coplanar conformation. This mechanism is evidenced by the concurrent recovery of the ground-state bleach of the planarized species and bleaching of ground state of the nonplanarized species. The third component corresponds to the excited-state decay of $^{1*}\mathbf{1}$ and $^{1*}\mathbf{2}$, as these ~1-ns components match the fluorescence lifetimes of $^{1*}\mathbf{1}$ and $^{1*}\mathbf{2}$ in toluene ($\tau = 1.2 \pm 0.1$ and 1.3 ± 0.1 ns, respectively), which were independently measured using a fluorescence lifetime apparatus having a 20-ps instrument response time (not shown).

The SAXS data shows that coordination of the dimers to the trigonal ligands ensures that the macrocycles that comprise each dimer are locked in their coplanar conformation without deformation of the butadiyne linkers. Assignment of the initial negative features in the transient absorption spectra of **1** and **2** to excitation of the coplanar dimers was confirmed by excitation of **1₃-SL₂** and **2₃-SL₂** in toluene with 710- and 730-nm, 120-fs pulses, respectively. Excitation of **1₃-SL₂** yields the transient absorption spectrum of $^{1*}\mathbf{1_3}\text{-}\mathbf{SL_2}$, with ground-state bleaching of the Q bands at 652, 675, and 713 nm, bleaching of the Soret band below 483 nm, and excited-state absorption between 483 and 633 nm, Figure 8. Excitation of **2₃-SL₂** yields the transient absorption spectrum of $^{1*}\mathbf{2_3}\text{-}\mathbf{SL_2}$ with ground-state bleaching of the Q-band at 732 nm, bleaching of the Soret band at 494 nm, and excited-state absorption between 510 and 692 nm, Figure 9. Transient kinetics for $^{1*}\mathbf{1_3}\text{-}\mathbf{SL_2}$, monitored at 721 nm, reveal three exponential decay components with lifetimes of

(39) Screen, T. E. O.; Thorne, J. R. G.; Denning, R. G.; Bucknall, D. G.; Anderson, H. L. *J. Mater. Chem.* **2003**, *13*, 2796–2808.

Figure 9. Transient absorption spectra of $2_3\text{-}\textbf{SL}_2$ in toluene following excitation with 730-nm, 120-fs laser pulses. Inset: Power-dependent transient absorption kinetics monitored at 740 nm using 1.00 (black), 0.66 (red), 0.33 (green), and 0.11 (blue) μJ per 730 nm excitation pulse.

Figure 10. Transient absorption spectra of $1_3\text{-}\textbf{LL}_2$ in toluene following excitation with 710-nm, 120-fs laser pulses. Inset: Power-dependent transient absorption kinetics monitored at 721 nm using 1.00 (black), 0.66 (red), 0.33 (green), and 0.11 (blue) μJ per 710 nm excitation pulse.
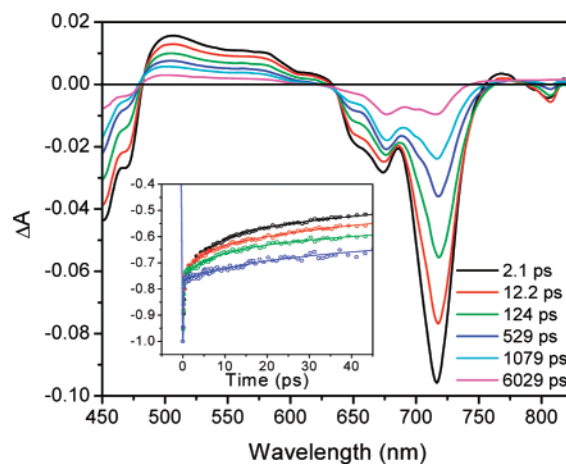

Figure 11. Transient absorption spectra of $2_3\text{-}\textbf{LL}_2$ in toluene following excitation with 730-nm, 120-fs laser pulses. Inset: Power-dependent transient absorption kinetics monitored at 740 nm using 1.00 (black), 0.66 (red), 0.33 (green), and 0.11 (blue) μJ per 730 nm excitation pulse.

0.31 ± 0.11 ps (0.43), 3.1 ± 0.1 ps (0.07), and 1.2 ± 0.1 ns (0.50), Figure 8 inset, and kinetics of $^{1*}2_3\text{-}\textbf{SL}_2$, monitored at 740 nm, also show three exponential decay components with lifetimes of 0.28 ± 0.05 ps (0.35), 2.4 ± 0.3 ps (0.09), and 1.4 ± 0.1 ns (0.56), Figure 9 inset. The relative amplitudes are given for the lowest laser pump energies as indicated in the figures.

The first component in the transient decays of both prisms is the result of the nonlinear decay process, and the $\sim$1 ns component is the result of excited-state decay, which matches the fluorescence lifetimes of $\tau = 1.2 \pm 0.1$ and 1.4 ± 0.1 ns for $^{1*}1_3\text{-}\textbf{SL}_2$ and $^{1*}2_3\text{-}\textbf{SL}_2$ in toluene, respectively, Figures S7 and S8. However, the second component, $\tau = 3.1$ and 2.4 ps for $^{1*}1_3\text{-}\textbf{SL}_2$ and $^{1*}2_3\text{-}\textbf{SL}_2$, respectively, is not the result of conformational dynamics as it was in the transient kinetics of **1** and **2**. The amplitudes of these components display a quadratic dependence on laser power indicative of singlet−singlet annihilation, insets in Figures 8 and 9.[25] Assuming annihilation is the result of random exciton transfer between adjacent dimeric chromophores, the time constants for exciton hopping within each prism, τ_h, can be derived from the annihilation lifetime, τ_a, using the formula

$$\tau_a = \frac{\tau_h}{8 \sin^2(\pi/2N)} \tag{1}$$

developed by Trinkunas for cyclic arrays of N chromophores.[40] Using this model, $N = 3$ and the measured values of τ_a and $\tau_h = 6.2 \pm 0.2$ and 4.8 ± 0.6 ps for $^{1*}1_3\text{-}\textbf{SL}_2$ and $^{1*}2_3\text{-}\textbf{SL}_2$, respectively. Due to the parallel orientation of the transition dipole moments along the butadiyne linkage of the dimers comprising each face of the prismatic assemblies, anisotropy measurements cannot be used to confirm the rates of energy transfer. To prove that singlet−singlet annihilation is the result of energy transfer between dimers in the prisms and not between chromophores within the dimers, transient absorption studies of the larger trigonal prisms are required.

Excitation of $1_3\text{-}\textbf{LL}_2$ and $2_3\text{-}\textbf{LL}_2$ in toluene with 710- and 730-nm, 120-fs pulses, respectively, reveals transient absorption spectra that are nearly identical with those obtained for $1_3\text{-}\textbf{SL}_2$ and $2_3\text{-}\textbf{SL}_2$ in toluene, Figures 10 and 11. Transient absorption

(40) Trinkunas, G. *J. Lumin.* **2003**, *102−103*, 532−535.
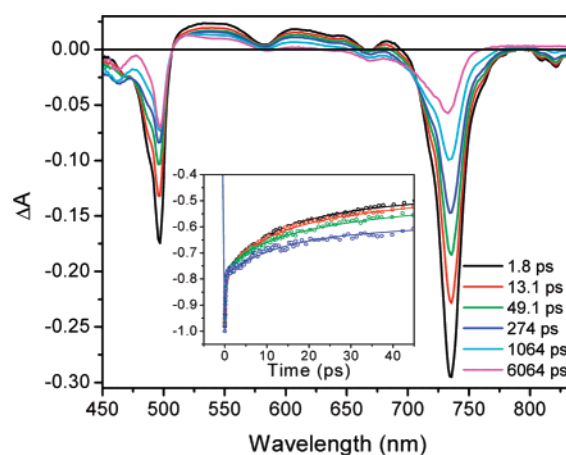
kinetics for $1_3\text{-}\textbf{LL}_2$, monitored at 721 nm, show 3 exponential decay components with lifetimes of 0.18 ± 0.05 ps (0.58), 7.3 ± 1.7 ps (0.08), and 1.1 ± 0.1 ns (0.34), respectively, Figure 10 inset, and kinetics of $2_3\text{-}\textbf{LL}_2$, monitored at 740 nm, show 3 similar exponential decay components with lifetimes of 0.13 ± 0.03 ps (0.78), 9.2 ± 1.0 ps (0.11), and 1.3 ± 0.1 ns (0.11), respectively, Figure 11. The $\sim$1 ns lifetimes are once again the result of excited-state decay, as corroborated by the fluorescence decay data presented in Figures S9 and S10, while the amplitudes of the 7.3 and 9.2 ps components depend quadratically on laser power indicative of singlet−singlet annihilation, insets in Figures 10 and 11.[25] Using the model described above, $N = 3$ and the measured values of τ_a and $\tau_h = 14.6 \pm 3.4$ and 18.4 ± 2.0 ps for $^{1*}1_3\text{-}\textbf{LL}_2$ and $^{1*}2_3\text{-}\textbf{LL}_2$, respectively. These laser power dependent components are longer relative to those of $1_3\text{-}\textbf{SL}_2$ and $2_3\text{-}\textbf{SL}_2$ and are consistent with the assignment of these components to singlet−singlet annihilation between excited dimers in the prisms.

Energy transfer between the dimers that comprise the faces of the prisms most likely occurs entirely through the Förster

Table 1. Fluorescence Data and Results of Förster-Type Energy Transfer Calculations for Prisms in Toluene

struct	λ_F	τ_F (ns)	$\Phi_F{}^a$	τ_h (ps)	R (nm)^b	κ^2	$\tau_{FRET}(S_1 \rightarrow S_1)$ (ps)	$\tau_{FRET}(S_1 \rightarrow S_0)$ (ps)
1_3-SL$_2$	733	1.19	0.07	6.2 ± 0.2	1.73	1	10.3	11.1
1_3-LL$_2$	737	1.10	0.08	14.6 ± 3.4	2.83	1	157	171
2_3-SL$_2$	749	1.36	0.14	4.8 ± 0.6	1.73	1	1.1	0.9
2_3-LL$_2$	749	1.33	0.15	18.4 ± 2.0	2.83	1	19.2	11.9

^{a} Fluorescence quantum yields use DOTC iodide[59] as a reference. ^{b} Values derived from MM+ geometry-optimized models obtained using Hyperchem.[37]

mechanism.[41−45] The competing Dexter mechanism[46] requires a direct orbital pathway between energy donors and acceptors,[47,48] so that contributions from the Dexter mechanism in the prismatic assemblies are most likely negligible because the large distance between the dimer faces prohibits overlap of the donor and acceptor orbitals. Overlap of the trigonal ligand orbitals and the dimer orbitals is also negligible due to the small orbital coefficient at the Zn centers of both tetrapyrrole macrocycles.[25,49]

The rate of Förster resonance energy transfer[41] is expressed as

$$k_{FRET} = 8.785 \times 10^{-11} \left(\frac{\kappa^2 \Phi_F}{n^4 R^6 \tau_F} \right) \int_{\Delta\lambda} f_D(\lambda) \lambda^4 \epsilon_A(\lambda) \, d\lambda \ (ps^{-1}) \ (2)$$

where κ^2 is the geometrical factor, n is the effective index of refraction (1.496 for toluene) used to determine the Coulombic interaction between the donor and the acceptor,[50] R (nm) is the distance between chromophores, $f_D(\lambda)$ is the corrected fluorescence intensity of the donor with the total intensity normalized to unity, $\epsilon_A(\lambda)$ is the extinction coefficient of the acceptor in $M^{-1} \ cm^{-1}$, and Φ_F and τ_F are the donor fluorescence quantum yield and lifetime, respectively. If singlet−singlet annihilation between a pair of chromophores that are both excited to their S_1 states occurs by Förster energy transfer,[51] calculating k_{FRET} using eq 2 requires the $S_1 \rightarrow S_0$ emission spectrum of the donor chromophore and the $S_1 \rightarrow S_n$ absorption spectrum of the acceptor chromophore.[52] However, if the number of chromophores in the ensemble increases beyond 2, the probability of having energy transfer occur between an excited chromophore and a nearby ground-state chromophore prior to singlet−singlet annihilation also increases. As a consequence, the overall exciton

hopping rate (τ_h) derived from eq 1 has an increasing contribution from energy transfer from an excited chromophore to one in its ground state. Therefore, using the $S_1 \rightarrow S_0$ emission spectrum of the donor chromophore and the $S_0 \rightarrow S_1$ absorption spectrum of the acceptor chromophore in eq 2 to calculate k_{FRET} becomes an increasingly better approximation as the number of chromophores over which the exciton hops increases.[53,54] For the prismatic chlorophyll and porphyrin assemblies studied here, there are only three chromophores/prism, so that when two S_1 states are present in each prism, each of them can hop either to one S_0 chromophore or to the other S_1 chromophore and annihilate. To determine the best approximation, we will calculate and compare both the $S_1 \rightarrow S_1$ and $S_1 \rightarrow S_0$ Förster energy transfer rates.

The ground-state absorption spectra of **1_3-SL$_2$**, **1_3-LL$_2$**, **2_3-SL$_2$**, and **2_3-LL$_2$** in toluene are presented in Figures 3 and 4, their fluorescence spectra are given in Figure S11, and their fluorescence maxima (λ_F), quantum yields (Φ_F), and lifetimes (τ_F) are listed in Table 1. For all molecules, the emission features are approximately mirror images of the corresponding $Q_y(0,0)$ and $Q_y(0,1)$ absorption features. The most prominent features in the transient absorption spectra of **1_3-SL$_2$**, **1_3-LL$_2$**, **2_3-SL$_2$**, and **2_3-LL$_2$** in toluene, Figures 8−11, are bleaches of their ground-state absorption bands and stimulated emission. The remaining absorption changes due to their $S_1 \rightarrow S_n$ transitions are broad and essentially featureless across most of the visible and near-infrared region.[55−57] Because it is difficult to accurately subtract the prominent stimulated emission features from the transient absorption spectra, we have approximated the $S_1 \rightarrow S_n$ spectra by using a constant value of the $S_1 \rightarrow S_n$ absorbance obtained from the transient absorption observed at 480−620 nm for **1_3-SL$_2$** and **1_3-LL$_2$** and 520−650 nm for **2_3-SL$_2$**, and **2_3-LL$_2$**, where their respective ground states have very little absorption. The estimated $S_1 \rightarrow S_n$ absorbance is assumed to be constant throughout the region of the $S_1 \rightarrow S_0$ emission from the donor. The time constants for Förster energy transfer ($\tau_{FRET} = 1/k_{FRET}$) were calculated using the PhotochemCAD software package[58] and are presented in Table 1. The estimated $S_1 \rightarrow S_n$ absorbance is an upper limit (see Figure S12 and Table S1),[55−57] so that if the actual spectral overlap is smaller, the calculated Förster energy transfer times are slower. This would result in

(41) Lakowicz, J. R. *Principles of Fluorescence Spectroscopy*; Kluwer: Dordrecht, The Netherlands, 1999.
(42) Bradforth, S. E.; Jimenez, R.; van Mourik, F.; van Grondelle, R.; Fleming, G. R. *J. Phys. Chem.* **1995**, *99*, 16179−16191.
(43) Hwang, I.-W.; Ko, D. M.; Ahn, T. K.; Yoon, Z. S.; Kim, D.; Peng, X.; Aratani, N.; Osuka, A. *J. Phys. Chem. B* **2005**, *109*, 8643−8651.
(44) Hwang, I.-W.; Park, M.; Ahn, T. K.; Yoon, Z. S.; Ko, D. M.; Kim, D.; Ito, F.; Ishibashi, Y.; Khan, S. R.; Nagasawa, Y.; Miyasaka, H.; Ikeda, C.; Takahashi, R.; Ogawa, K.; Satake, A.; Kobuke, Y. *Chem.—Eur. J.* **2005**, *11*, 3753−3761.
(45) Hwang, I.-W.; Yoon, Z. S.; Kim, J.; Kamada, T.; Ahn, T. K.; Aratani, N.; Osuka, A.; Kim, D. *J. Photochem. Photobiol., A* **2006**, *178*, 130−139.
(46) Dexter, D. L. *J. Chem. Phys.* **1953**, *21*, 836−850.
(47) Closs, G. L.; Piotrowiak, P.; MacInnis, J. M.; Fleming, G. R. *J. Am. Chem. Soc.* **1988**, *110*, 2652−2653.
(48) Closs, G. L.; Johnson, M. D.; Miller, J. R.; Piotrowiak, P. *J. Am. Chem. Soc.* **1989**, *111*, 3751−3753.
(49) Yatskou, M. M.; Koehorst, R. B. M.; van Hoek, A.; Donker, H.; Schaafsma, T. J.; Gobets, B.; van Stokkum, I.; van Grondelle, R. *J. Phys. Chem. A* **2001**, *105*, 11432−11440.
(50) Knox, R. S.; van Amerongen, H. *J. Phys. Chem. B* **2002**, *106*, 5289−5293.
(51) Agranovich, V. M.; Galanin, M. D. *Electronic Excitation Energy Transfer in Condensed Media*; Elsevier: Amsterdam, 1982.
(52) Larsen, J.; Bruggemann, B.; Polivka, T.; Sundstrom, V.; Akesson, E.; Sly, J.; Crossley Maxwell, J. *J. Phys. Chem. A* **2005**, *109*, 10654−10662.
(53) Barzda, V.; Gulbinas, V.; Kananavicius, R.; Cervinskas, V.; van Amerongen, H.; van Grondelle, R.; Valkunas, L. *Biophys. J.* **2001**, *80*, 2409−2421.
(54) Valkunas, L.; Trinkunas, G.; Liuolia, V.; van Grondelle, R. *Biophys. J.* **1995**, *69*, 1117−1129.
(55) Baugher, J.; Hindman, J. C.; Katz, J. J. *Chem. Phys. Lett.* **1979**, *63*, 159−162.
(56) Shepanski, J. F.; Anderson, R. W., Jr. *Chem. Phys. Lett.* **1981**, *78*, 165−173.
(57) Becker, M.; Nagarajan, V.; Parson, W. W. *J. Am. Chem. Soc.* **1991**, *113*, 6840−6848.
(58) Du, H.; Fuh, R.-C. A.; Li, J.; Corkan, L. A.; Lindsey, J. S. *Photochem. Photobiol.* **1998**, *68*, 141−142.

an even wider divergence between the calculated energy transfer times and the experimentally determined values of τ_h given in Table 1.

It is interesting to note that the calculated values of τ_{FRET} for both $S_1 \rightarrow S_1$ and $S_1 \rightarrow S_0$ Förster energy transfer agree to within a factor of 2. This is most likely a consequence of the comparable degree of overlap between the $S_1 \rightarrow S_0$ emission spectrum and both the $S_1 \rightarrow S_n$ and $S_0 \rightarrow S_1$ absorption spectra for these chromophores, which has been discussed previously for chlorophylls.[53] This suggests that, for chromophore ensembles of chlorophylls or porphyrins, either method of calculating τ_{FRET} gives a reasonable benchmark to compare with experimentally determined hopping rates. However, this fortuitous similarity in spectral overlap is not generally true for other chromophores.

The relative ratios of the experimental exciton hopping rates, τ_h, between the chromophore faces in the larger prisms and in the smaller prisms are about 2:1 and 4:1 for the chlorophyll and the porphyrin faces, respectively. The analogous ratios of τ_{FRET} are approximately 15:1 for both the chlorophyll and the porphyrin faces, irrespective of the method used to calculate τ_{FRET}. This discrepancy most likely stems from the breakdown of the point−dipole approximation used in the formulation of the Förster theory. The extent of the transition dipole moments in both the chlorophyll and porphyrin dimers is comparable to the distances between the faces of the prisms comprised of them. Several studies involving conducting polymers[60,61] and multi-chromophoric dendrimers[62,63] have shown the inadequacy of the point−dipole approximation when the distance between the energy donors and acceptors in a system are similar to the overall length of the transition dipole moments of the component chromophores. As a result, several computational methods have recently emerged in an attempt to find better agreement between the experimentally observed energy transfer rates and those obtained from theoretical methods.[64−69] Future studies of these assemblies will involve applying these methods.

Conclusions

The butadiyne linkages between chlorophyll chromophores in **1** and between the porphyrin chromophores in **2**[3−5,9,22] result

in significant spectral enhancements due in part to the reduction in symmetry of the component chromophores and electronic delocalization that lengthens the transition dipole. By restriction of these dimers to structurally rigid, prismatic structures, by the addition of 2/3 equiv of a trigonal bridging ligand, the factors contributing to the spectral enhancements are accentuated. Power-dependent transient absorption measurements on the prisms with different chromophore−chromophore distances identified one of the decay components in the transient absorption kinetics as resulting from singlet−singlet annihilation. From the annihilation kinetics, we are able to obtain the lifetimes of exciton migration between the dimers which comprise the faces of the prisms. Due to the similarity of the exciton migration lifetimes between chlorophyll and porphyrin dimer prisms with the same size trigonal ligand, it appears as though the energy transfer rates are independent of the chromophores from which the butadiyne dimers were synthesized. This independence is indicative of the fact that energy transfer occurs from the low-energy transition situated along the long axis of the dimers and that these transitions for both chlorophylls and porphyrins have similar energies. This work provides an example of structural control over photophysical processes, knowledge of which is crucial for the design of future photofunctional materials for solar energy conversion.

Supporting Information Available: Experimental details including the synthesis and characterization of the dimers and prisms, fluorescence spectra, time-resolved fluorescence data, additional small-angle X-ray scattering data, and Förster energy transfer calculations. This material is available free of charge via the Internet at http://pubs.acs.org.

JA075494F

(59) Sanyal, S.; Akselrod, M. S. *J. Appl. Phys.* **2005**, *98*, 033518/033511−033518/033512.

(60) Cornil, J.; Beljonne, D.; Friend, R. H.; Bredas, J. L. *Chem. Phys. Lett.* **1994**, *223*, 82−88.

(61) Pichler, K.; Halliday, D. A.; Bradley, D. D. C.; Burn, P. L.; Friend, R. H.; Holmes, A. B. *J. Phys.: Condens. Matter* **1993**, *5*, 7155−7172.

(62) Flors, C.; Oesterling, I.; Schnitzler, T.; Fron, E.; Schweitzer, G.; Sliwa, M.; Herrmann, A.; Van der Auweraer, M.; De Schryver, F. C.; Müllen, K.; Hofkens, J. *J. Phys. Chem. C* **2007**, *111*, 4861−4870.

(63) Fron, E.; Flors, C.; Schweitzer, G.; Habuchi, S.; Mizuno, H.; Ando, R.; De Schryver, F. C.; Miyawaki, A.; Hofkens, J. *J. Am. Chem. Soc.* **2007**, *129*, 4870−4871.

(64) Krueger, B. P.; Scholes, G. D.; Fleming, G. R. *J. Phys. Chem. B* **1998**, *102*, 5378−5386.

(65) Krueger, B. P.; Scholes, G. D.; Fleming, G. R. *J. Phys. Chem. B* **1998**, *102*, 9603.

(66) Reimann, C. T.; Velazquez, I.; Tapia, O. *J. Phys. Chem. B* **1998**, *102*, 9344−9352.

(67) Wong, K. F.; Bagchi, B.; Rossky, P. J. *J. Phys. Chem. A* **2004**, *108*, 5752−5763.

(68) Ortiz, W.; Krueger, B. P.; Kleiman, V. D.; Krause, J. L.; Roitberg, A. E. *J. Phys. Chem. B* **2005**, *109*, 11512−11519.

(69) Jean, J. M.; Krueger, B. P. *J. Phys. Chem. B* **2006**, *110*, 2899−2909.